Invited Paper

Laser diode interferometers equipped with an electrical feedback loop

Takamasa Suzuki* and Osami Sasaki

Niigata University, Faculty of Engineering
8050 Ikarashi 2, Niigata City, 950-2181, Japan

ABSTRACT

The tunability of the laser diode's operative wavelength is very attractive to realize active interferometer. We review here, a system that possesses this important capability, by virtue of its built-in electrical feedback loop. After describing the basic principles of its phase-control and feedback-signal generation, some selected examples of its implementation, such as displacement-, profile- and distance-measurements, as well as disturbance elimination are presented.

Keywords: interferometry, laser diode, feedback control, phase-locked technique, sinusoidal phase modulation

1. INTRODUCTION

In the mid nineteen-eighty's, when the science of laser diode (LD) interferometry was in its infancy, researchers were forced to rely on cumbersome, low-efficiency gas lasers as light-sources. Fifteen years of evolution have produced small, lightweight, highly efficient apparatus, whose laser-diode wavelengths can be fine-tuned, and whose interference-signal phase is modulated, through simple adjustments of the injection-current[1-3]. The wavelength tunability allows us to combine interferometer with an electronic circuit and to construct an active interferometers; - something that would be impossible to construct by use of the conventional gas lasers. Of all the LD interferometers currently available, one of the most important is the feedback (FB) type of interferometer that uses electrical FB technique[3]. In such interferometers, the FB control is used for measurement[4-6] itself and /or elimination of the external disturbances[7].

2. PRINCIPLE OF PHASE-CONTROL IN LD INTERFEROMETERS

The block diagram in Fig. 1 presents a typical FB LD interferometer, equipped with electronic system. The LD acts as the common and key device, in both systems. The LD's injection current, which is produced by the LD modulator (LM), consists of dc bias current I_0, modulation current $\Delta i_m(t)$, and control current $\Delta i_c(t)$. The central wavelength λ_0 is determined by I_0. The laser beam radiating from the LD is fed into the interferometric optical system (OPT), which, in turn, generates the interference signal that transmits data regarding the object's displacement, vibration, and physical profile. A photodetector (PDT) generates an electrical interference signal. We commonly use a photodiode (PD) or a CCD image sensor as the PDT. PDs detect even the slightest temporal displacement or vibration, while CCD image sensors provide one- or two-dimensional profiles. The FB signal generator (FBSG) extracts the FB signal, which contains information relating to phase deviation, from the interference signal detected by the PDT. The feedback controller (FBC) generates the control current, in order to compensate for phase deviation. The spatio-temporal interference signal is represented by

$$S(t,x,y) = S_1 + S_0 \cos\alpha(t,x,y), \qquad (1)$$

where

$$\alpha(t,x,y) = \alpha_0 + \alpha_d(t) + \alpha_p(x,y), \qquad (2)$$

* Correspondence: E-mail: takamasa@eng.niigata-u.ac.jp; phone/fax: +81-25-262-7215;
Niigata University, 8050 Ikarashi 2, Niigata, 950-2181 JAPAN

Advanced Materials and Devices for Sensing and Imaging, Jianquan Yao, Yukihiro Ishii, Editors, Proceedings of SPIE Vol. 4919 (2002) © 2002 SPIE · 0277-786X/02/$15.00

$\alpha_0=2\pi L_0/\lambda_0$ is the initial phase,

$$\alpha_d(t)=\frac{2\pi d(t)}{\lambda_0} \tag{3}$$

is the temporally varying phase, and

$$\alpha_p(x,y)=\frac{2\pi H(x,y)}{\lambda_0} \tag{4}$$

is the spatially varying one, respectively. S_1 and S_0 refer to the dc component and the amplitude of the ac component, respectively. L_0, d(t), and H(x, y), represent the initial optical path difference (OPD), as well as momentary changes in the OPD, and the surface profile.

As wavelength of the LD linearly varies with the injection current, wavelength fluctuation is given by[1]

$$\Delta\lambda(t)=\beta\Delta i(t), \tag{5}$$

where we refer to, as proportional constant β as the modulation efficiency. If we increase λ_0 by $\Delta\lambda_d(t)=\beta\Delta i_d(t)$, for d(t) and by $\Delta\lambda_p(x, y)=\beta\Delta i_p(t)$, for H(x, y), Eq. (2) is rewritten as:

$$\alpha_0+[\alpha_d(t)-\Delta\alpha_d(t)]+[\alpha_p(x,y)-\Delta\alpha_p(x,y)], \tag{6}$$

where

$$\Delta\alpha_d(t)=\frac{2\pi L_0}{\lambda_0^{\,2}}\beta\Delta i_d(t). \tag{7}$$

and

$$\Delta\alpha_p(x,y)=\frac{2\pi L_0}{\lambda_0^{\,2}}\beta\Delta i_p(x,y). \tag{8}$$

This would indicate that the LD interferometer's phase could be controlled, through slight adjustments of the injection current. In the FB interferometer, we usually set the second or third term in Eq. (6) to zero. $\Delta i_d(t)$ or $\Delta i_p(x, y)$ is automatically determined by the FB control. (See schematic, Fig. 2.) When the phase deviates from its normal state, it is immediately compensated for, by the FB control. We refer to the location of $\alpha_d(t)$ or $\alpha_p(x, y)$ as the "operating point", which decides the type of the FB control[8]. When the operating point lies in the (A) region, a negative feedback is

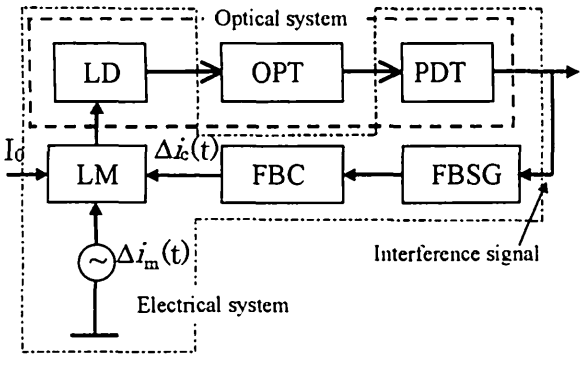

Fig. 1 Feedback type of laser diode interferometer.

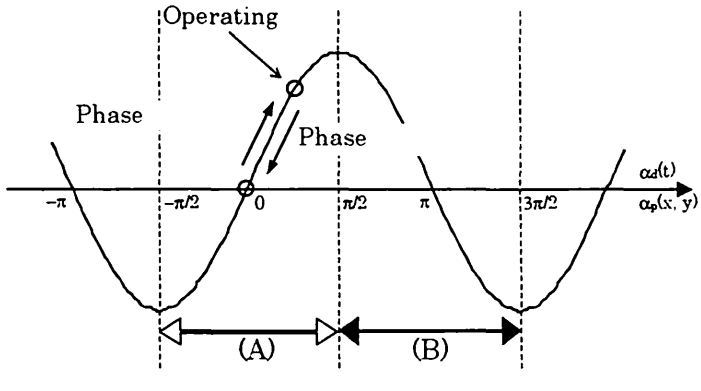

Fig. 2 Schematic of the feedback control.

achieved, whereas its location in the (B) region would result in positive feedback. If the operating point is in the (B) region, it moves to the region (A) so as to stabilize the FB loop itself, and the feedback loop is settled.

3. GENERATION OF THE FB SIGNAL

In the FB interferometer, it is very important to generate the FB signal which contains the phase we want to control. There are three main types of interferometry that are classified according to modulation signal. Figure 3 shows their waveforms and corresponding interference signals. When the modulating signal $\Delta i_m(t)$ is injected into the LD, the wavelength changes by $\Delta\lambda_m(t)=\beta\Delta i_m(t)$. Thus, the initial phase a_0 varies as

$$\frac{2\pi L_0}{\lambda_0-\beta\Delta i_m(t)}=\alpha_0+\Delta\alpha_m(t), \tag{9}$$

where

$$\Delta\alpha_m=\frac{2\pi L_0\beta}{\lambda_0}\Delta i_m(t). \tag{10}$$

In phase-shifting interferometry[2, 9], the modulating signal fluctuates by degrees, as shown in Fig. 3(a). The interference signal is then given by

$$S(t,x,y)=S_1+S_0\cos\left[(i-1)\pi/2+\alpha_d(t)+\alpha_p(x,y)\right], \tag{11}$$

where i=1-4. As the interference fringe is stationary at each step, we can generate an FB signal

$$F_1(t)=S_1+S_0\cos[(i-1)\pi/2+\alpha(t)+\alpha(x_0, y_0)] \tag{12}$$

using the PD and a pinhole, where (x_0, y_0) denotes the fixed point observed by the PD. The FB signal $F_1(t)$, however, contains dc component S_1.

A spatial filtering detector (SFD) can be used instead of the PD. This devise has a periodic array of PDs with mutual connections. The output signal is proportional to the fringe shift. Active phase shifting LD interferometer equipped with the SFD has been proposed[10, 11].

Heterodyne interferometers' modulation signals are triangular[1, 12] (Fig. 3(b)). When the inclination of a slope is γ, the interference signal detected by the PD is given by

$$S(t,x,y)=S_1+S_0\cos[2\pi ft+\alpha(t)+\alpha(x_0,y_0)], \tag{13}$$

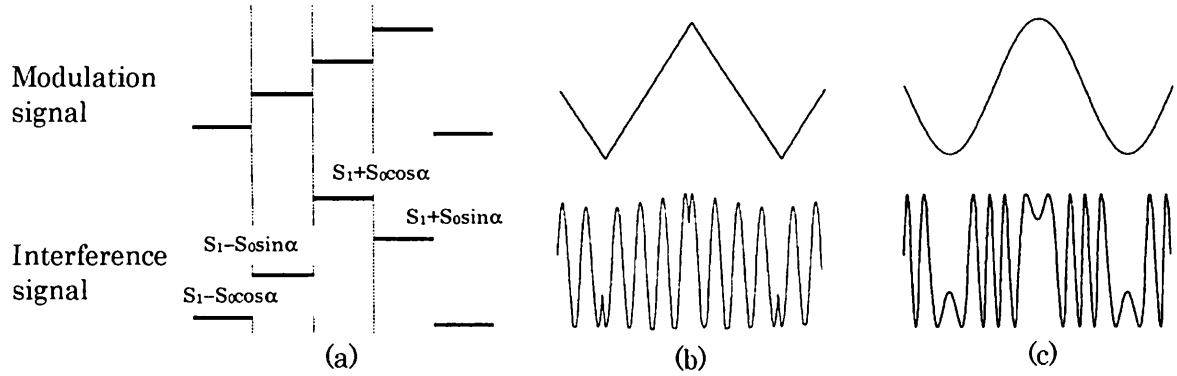

Fig. 3 Interferometries classified by the modulation signal: (a) phase shifting LD interferometry, (b) heterodyne LD interferometry, and (c) sinusoidal phase modulating LD interferometry.

where

$$f = \frac{\gamma\beta}{\lambda_0} L_0 . \tag{14}$$

Interference signal becomes discontinuous and sinusoidal in nature, with a signal whose frequency is constant. As the interference signal is not stationary, we sample and hold it at the constant phase of the modulation signal, and convert it to a continuous one[13], using the low-pass filter (LPF). We then obtain

$$F_2(t)=S_1+S_0\cos\alpha(t) \tag{15}$$

as the FB signal.

When we use sinusoidal signal

$$\Delta i_m(t) = a\cos(\omega_c t+\theta) \tag{16}$$

as the modulating signal (Fig. 3(c)), we can obtain sinusoidal phase modulating (SPM) signal[7]

$$\begin{aligned} S(t,x,y) &= S_1 + S_0\cos[z\cos(\omega_c t+\theta)+\alpha(t,x,y)] \\ &= S_1 + S_0\cos\alpha(t,x,y)[J_0(z)-2J_2(z)\cos 2(\omega_c t+\theta)+\cdots], \\ &\quad -S_0\sin\alpha(t,x,y)[2J_1(z)-2J_3(z)\cos 3(\omega_c t+\theta)+\cdots] \end{aligned} \tag{17}$$

where $J_n(z)$ is the n-th order Bessel function and

$$z = \frac{2\pi a\beta}{\lambda_0^2} L_0 \tag{18}$$

is the modulation depth. While the frequency of the SPM interference signal is not constant, it does contain higher modulating-frequency components, and can accommodate high-speed phase modulation.

So, of the two methods proposed for generating the FB signal in SPM interferometry, the first uses synchronous detection[14], and is applicable when a PD is used as the PDT; multiplying S(t, x, y) by $\Delta i_m(t)$ and passing it through the LPF, we obtain the signal

$$F_3(t)=A_s\sin\alpha(t) \tag{19}$$

associated with the frequency component of ω_c, where $A_s=-2KS_0aJ_1(z)$ and K is the gain of the LPF. The second method takes advantage of the CCD image sensor's ability to detect interference signals[15]; we synchronize the CCD image-sensor with modulation current $\Delta i_m(t)$. When signal S(t, x, y) is integrated during a quarter-period of $\Delta i_m(t)$, we obtain four images

$$p_i(x,y) = \int_{(T/4)(i-1)}^{(T/4)i} S(t,x,y)dt , \tag{20}$$

where $T=2\pi/\omega_c$. Calculating Eq. (20), and either adding or subtracting for each pixel, we easily obtain

$$P_s(x,y) = p_1 + p_2 - p_3 - p_4 = A_s\sin\alpha(x,y) , \tag{21}$$

and

$$P_c(x,y) = p_1 - p_2 + p_3 - p_4 = A_c\cos\alpha(x,y) , \tag{22}$$

where A_s and A_c are the functions of z and θ. They are given by

$$A_s = (8/\pi)\sum_{n=1}^{\infty}[J_{2n-1}(z)/(2n-1)](-1)^n \sin[(2n-1)\theta], \qquad (23)$$

$$A_c = (8/\pi)\sum_{n=1}^{\infty}[J_{2n}(z)/2n][1-(-1)^n]\sin(2n\theta). \qquad (24)$$

Signals $P_s(x, y)$ and $P_c(x, y)$ are then obtained from the CCD image sensor. The signals shown in Eqs. (12), (15), (19), (21), and (22) are easily applicable to the FB controls.

4. IMPLEMENTATIONS OF THE FB CONTROL

4.1 FB CONTROL FOR THE MEASUREMENT OF OPD'S CHANGE

To simplify the explanation, we assume $\Delta\alpha_p(x, y)$ to equal zero. With d(t) representing external disturbance, $\alpha_d(t)$ is targeted for elimination. Control-current $\Delta i_d(t)$ is automatically generated by the FBC and injected into the LD. Thus, the deviated phase $\alpha_d(t)$ is compensated and the second term in Eq. (6) is canceled. In this FB control, the FB signals shown in Eqs. (12), (15), or (19) are used. A proportional (P) control is usually sufficient to eliminate external disturbance. If we consider d(t) as a vibration of the object, we can measure it by observing the control current. Since the second term in Eq. (6) becomes zero when full compensation is achieved, we can derive

$$d(t) = \frac{L_0}{\lambda_0}\beta\Delta i_d(t) \qquad (25)$$

from Eqs. (3) and (7).

4.2 FB control for the measuerment of sureface profile

The implementation of FB control at each observation point allows us to accurately measure surface profile. FB signals similar to those in Eq. (21) or (22) are usually used; H(x, y) varies according to the results of surface-scans of the object, corresponding phase $\alpha_p(x, y)$ changes (Eq. (4)). When FB control completely compensates for these phase-changes, the third term in Eq. (6) becomes zero. Thus, the profile H(x, y) is given by

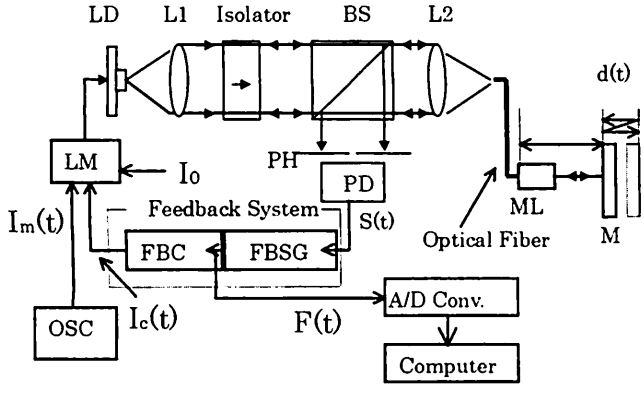

Fig. 4 Setup for the displacement measurement.

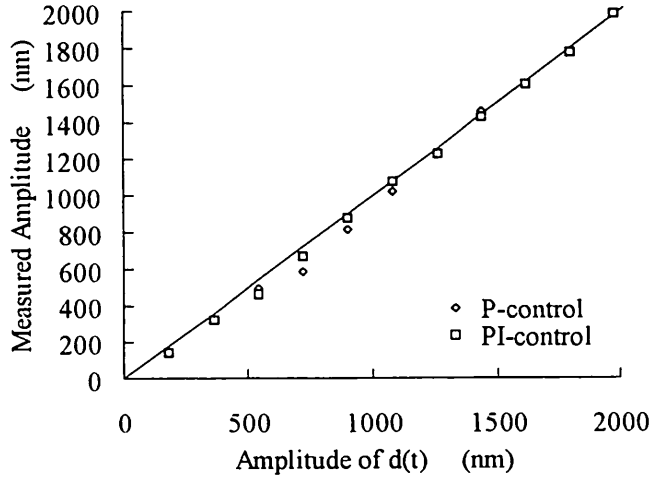

Fig. 5 Results of the sinusoidal-displacement measurement.

$$H(x,y)=\frac{L_0}{\lambda_0}\beta\Delta i_p(x,y) \qquad (26)$$

from Eqs. (4) and (8). The control current required in the compensation represents the surface profile. This is what we refer to as the "phase-locked" technique[4-6]. Here, the feedback control requires a proportional-integral (PI) control, so that phase deviations will be compensated with no offset errors.

5. SOME EXAMPLES OF THE MEASUREMENTS WITH THE FB CONTROL

5.1 DISPLACEMENT MEASUREMENT

Displacement measurement using FB LD interferometers was first reported more than fifteen years ago[3]. The interference signals were fed into the LD and measured the sinusoidal vibration whose amplitude was 4 μm. Another displacement measurement[16] is shown in Fig. 4. This one uses an optical fiber to measure the vibration of objects that cannot be moved onto the optical bench. The light from the LD is collimated with lens L1 and passed through an optical isolator, a beam-splitter (BS), and an optical fiber. The portion of the beam passing through the fiber is reflected back from the exit face, and is used as a reference beam. The output beam from the fiber is collimated with a micro lens (ML). It irradiates the object mirror (M). Therefore, a Fizeau interferometer is constructed in this optical system. The signal S(t) is fed in sequence to the LD, first, through a FB system and then, the LM to compensate for the phase-change caused by the vibration d(t) of the object. We used sinusoidal current for the modulation. We then have the FB signal of $F_3(t)=A_s\sin\alpha(t)$. The LD's wavelength λ_0, the modulation efficiency β, the OPD L_0, and the modulation frequency $2\pi/\omega_c$ were 670 nm, 4.0×10^{-3} nm/mA, $2D_0$=200mm, and 10kHz, respectively. The frequency response of the FB control mainly depends on the cut-off frequency of the LPF. It was no higher than 400 H. The M was driven by PZT having a sinusoidal signal of 100 Hz. Vibration amplitudes, which incidentally agree quite well with a theoretical solid line, were measured using the P- and PI-controls (Fig. 5). Both control systems proved to be accurate within 40 nm rms. From the FB loop's calculated gain, we were able to confirm the relationship between amplitude d(t) and the FB signal, to be d [nm]=217.3×F_3 [V]. Maximum, measurable amplitude equaled 1440 nm, in the P-control, but extended to 2000 nm, in the PI-control.

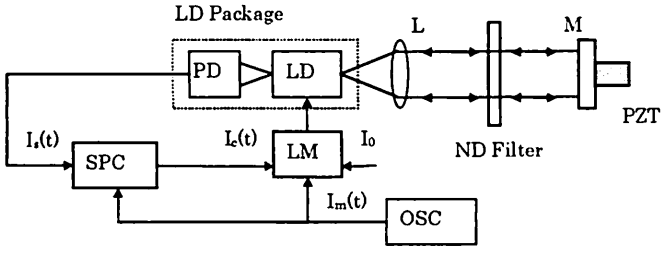

Fig. 6 Self-mixing type of LD interferometer.

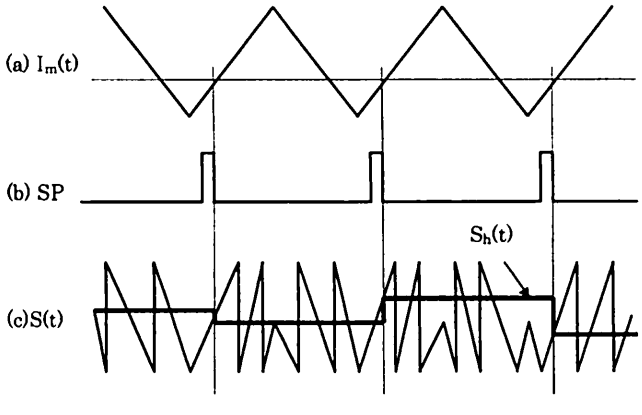

Fig. 7 Schematic of the FB signal generation by use of the sampling technique.

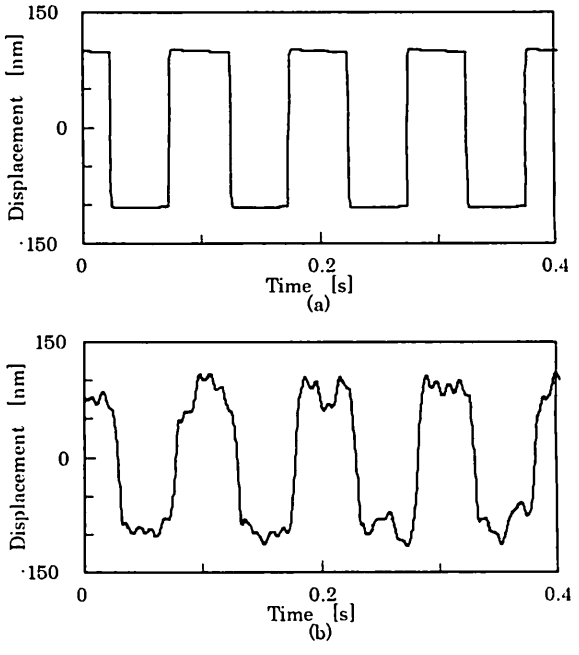

Fig. 8 Rectangular-displacements (a) calculated with the PZT's driving signal and (b) measured with self-mixing LD interferometer.

The FB control reduces phase-variation caused by d(t) to 1/23. Phase deviation resulting from external disturbance is suppressed to the same degree.

Another example of the displacement system is shown in Fig. 6. This one uses the self-mixing interferometer as an optical system. Since this setup does not require a beam-splitter, reference mirror, and external PD, the optical system is very simple, compared with conventional interferometers. For displacement measurement, the signal shown in Eq. (15) is used as the FB signal. This signal is generated, as shown in Fig. 7. The interference signal S(t) is sampled and held at the specific phase of the modulating current. The step-shaped signal $S_h(t)$ is fed into the LPF so as to generate the FB signal shown in Eq. (15). Measurement results are shown in Fig. 8. The upper trace pinpoints the PZT drive signal, while the lower one gives the displacement, as measured in real time. Parameters used in this measurement were λ_0=785 nm, β=2.0×10^{-3} nm/mA, L_0=400 mm, and $2\pi/\omega_c$=1 kHz. The formula shown in Eq. (25) was applied to this measurement.

5.2 SURFACE PROFILE MEASUREMENT

FB controls can be easily adapted for use in measuring surface profiles. Here, the phase-locked technique is particularly useful. Figure 9 shows an example of the phase-locked laser diode (PLLD) interferometer[5]. We injected SPM current $I_m(t)$ into the LD. As it uses a one-dimensional CCD image sensor, we considered only the x-direction. When we scan the measuring point, on the surface of the object, the phase $\alpha_p(x)$ varies according to the surface profile. We scanned 50 pixels, at intervals of 4 ms. If the FB control is achieved, such that the deviated phase is compensated, the surface profile H(x) is given by Eq. (26). Figure 10 shows the surface of the diamond-turned aluminum disk to vary by as much as 100 nm. We used signal $P_s(x)$ shown in Eq. (21) as the FB signal. Parameters in this measurement were λ_0=789 nm, β=6.0×10^{-3} nm/mA, L_0=100 mm, and $2\pi/\omega_c$=10 kHz, respectively. Roughness and cutting pitch agreed well with the result measured with a Talystep profiler. Measurement repeatability was less than 10 nm. At the same time, we observed the FB signal, which is shown in Fig. 11. It indicates that phase-locking is achieved in such a way that the FB signal is essentially zero, during the 4 ms scan.

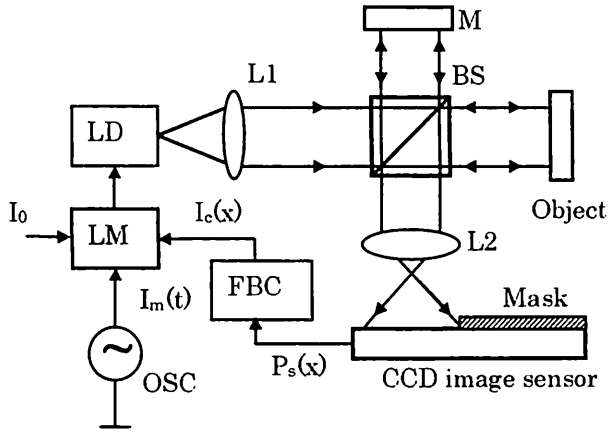

Fig. 9 Phase-locked laser diode interferometer.

PLLD interferometers' susceptibility to external disturbance stems from the fact that their FB controls are more suited to the implementation of phase locking. Another idea to eliminate the disturbance is the incorporation of differential detection[6]. A block diagram of the FBC in such system is shown in Fig. 12.

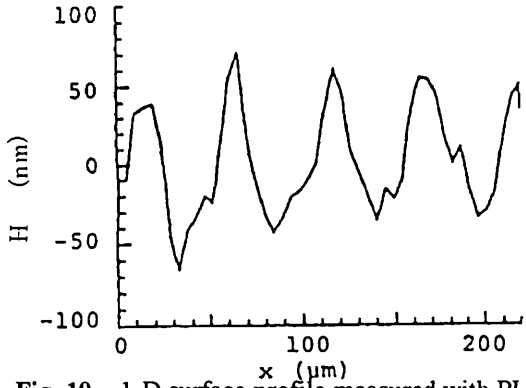

Fig. 10 1-D surface profile measured with PLLD interferometer.

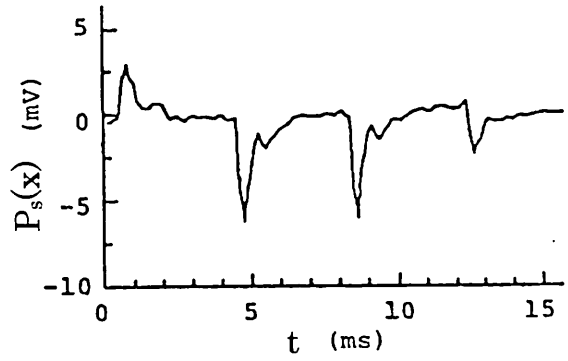

Fig. 11 Temporal change of the feedback signal in PLLD interferometer.

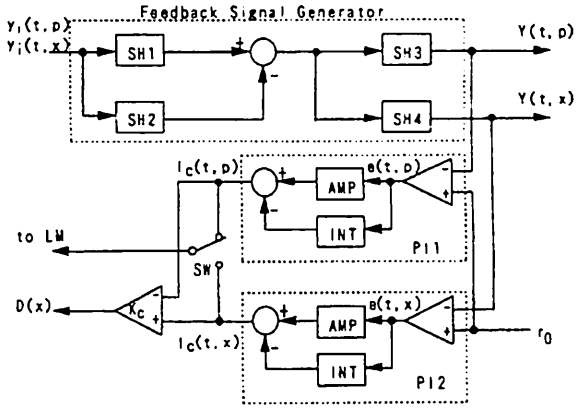

Fig. 12 Differential type of PLLD interferometer.

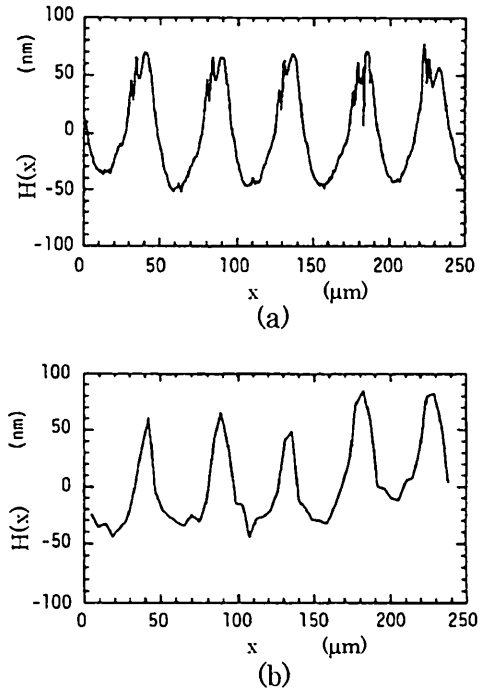

Fig. 13 1-D surface profile measured with (a) Talystep profiler and (b) differential type of PLLD interferometer.

While the experimental setup is the same as that shown in Fig. 9, control currents $I_c(t,p)$ and $I_c(t,x)$ are alternately injected into the LD. The compensating signal is held in the integrators (INTs) in PI1 and PI2, even if the SW is switched over. $I_c(t,p)$ and $I_c(t,x)$ are obtained, as fixed, and scanned measurement points, respectively. Feeding $I_c(t,p)$ and $I_c(t,x)$ into a differential amplifier whose gain is $L_0\beta/\lambda_0$, surface profile H(x) is obtained in real time. The experiment was implemented under the condition of λ_0=790nm, β=6.0×10^{-3} nm/mA, L_0=100 mm, and $2\pi/\omega_c$=7 kHz, respectively. Measurement results are shown in Fig. 13. The repeatability of 5 nm was confirmed, from several measurements.

5.3 DISTANCE MEASUREMENT

PLLD interferometry can also be applied to distance-measurement. One example[17] is shown in Fig. 14. Because we used a one-dimensional CCD image-sensor in this setup, the phase depends on the x-coordinate. We first prepare four quadratic signals $P_c(x)$, $P_s(x)$, $-P_c(x)$ and $-P_s(x)$, as shown in Fig. 15. When the wavelength of the LD is controlled, such that $P_c(x)=0$, the phase is locked at α_1. If the FB signals are successively changed from (a) to (e) by use of phase-locked technique, as shown in Fig. 15, the phase is finally locked at α_2. Thus, the phase accurately increases by 2π and we arrive at

$$\alpha_1(x)=2\pi L_0(x)/\lambda_1, \tag{27}$$

and

$$\alpha_2(x)=2\pi L_0(x)/\lambda_2, \tag{28}$$

where $\lambda_k=\lambda_0-\beta\Delta i_k$. As the difference between $\alpha_1(x)$ and $\alpha_2(x)$ is 2π, the OPD is given by

$$L_0(x)=\lambda_1\lambda_2/(\lambda_1-\lambda_2)$$

$$=\lambda_0^2/\beta(i_1-i_2). \tag{29}$$

That is to say, we can implement so-called two-wavelength interferometry, with just one LD.

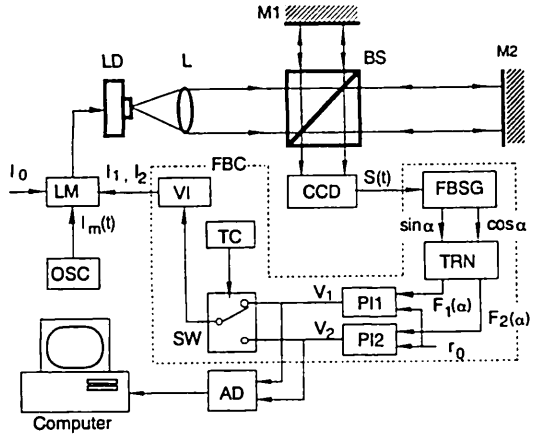

Fig. 14 Wavelength multiplexed LD interferometer for distance measurement.

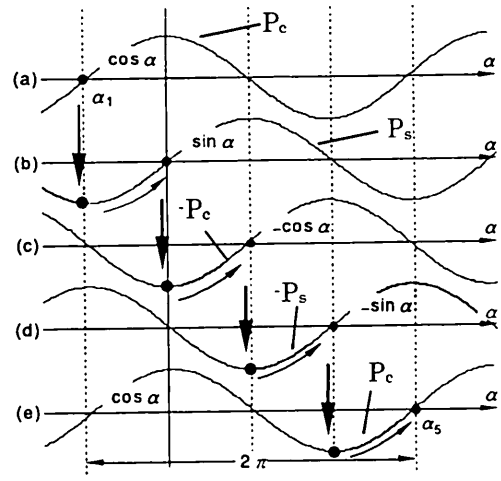

Fig. 15 Schematic of the phase-shifting with the feedback control.

We measured step-height, in one dimension, using a ~2 mm gauge block positioned at a distance of ~40 mm. Parameters used in this experiment were λ_0=780 nm, β=6.8×10^{-3} nm/mA, L_0=80 mm, and $2\pi/\omega_c$=2 kHz. In Fig. 16, circles indicate measured values. These are interpolated with a solid line. Distance was measured along the x-axis, in discrete 14-mm increments. The measurement error along the x-axis was estimated to be 0.16 mm rms.

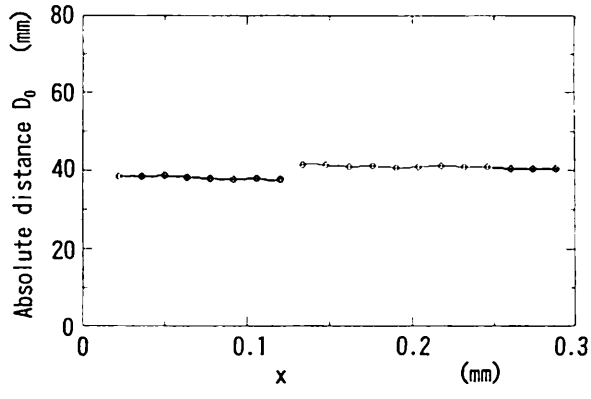

Fig. 16 Measured step-height of the gauge block whose thickness was ~2 mm.

Since the current range providing the linear wavelength is restricted to ~10 mA, the minimum L_0 becomes ~8.95 mm theoretically from Eq. (29). In the SPM interferometry, however, we need a longer OPD, to realize the appropriate modulation depth of z=2.45, with a small modulation current that does not induce the intensity modulation. Therefore, the minimum range of the OPD is actually 80 mm, in this type of LD interferometer. On the other hand, the maximum range depends on the device's ability to detect i_1-i_2. If we assume it measures 0.01 mA, the maximum range of the OPD becomes 8.95 m. This value, however, is restricted by the coherence of the LD used.

6. ELIMINATION OF THE EXTERNAL DISTURBANCE WITH THE FB CONTROL

6.1 DISTURBANCE-FREE PSI

The phase of the interference signal can be locked at specific values; a feature that is extremely useful, in phase-shifting LD interferometers. The setup[18] (Fig. 17) consists of three parts. In a typical photothermal modulating system[19], the source laser diode (LD1) is injected only with dc bias current. The sinusoidal intensity-modulated laser beam emitted from LD2 is fed into LD1 through the exit pupil and heats the laser chip in LD1. While the wavelength of LD1 is modulated via this temperature change, its output power displays little fluctuation. This is referred to as photothermal modulation. In the feedback control system, mirror M vibrates according to the sinusoidal signal. The interference signal is detected by the PD. Four quadratic signals for the phase shift are generated with the synchronous detection that has been shown in Eq. (19). The phase of the interference signal is then shifted as shown in Fig. 15. Accurate phase shift and disturbance elimination were achieved by the FB control. In the fringe analyzing system, the OPD was equal

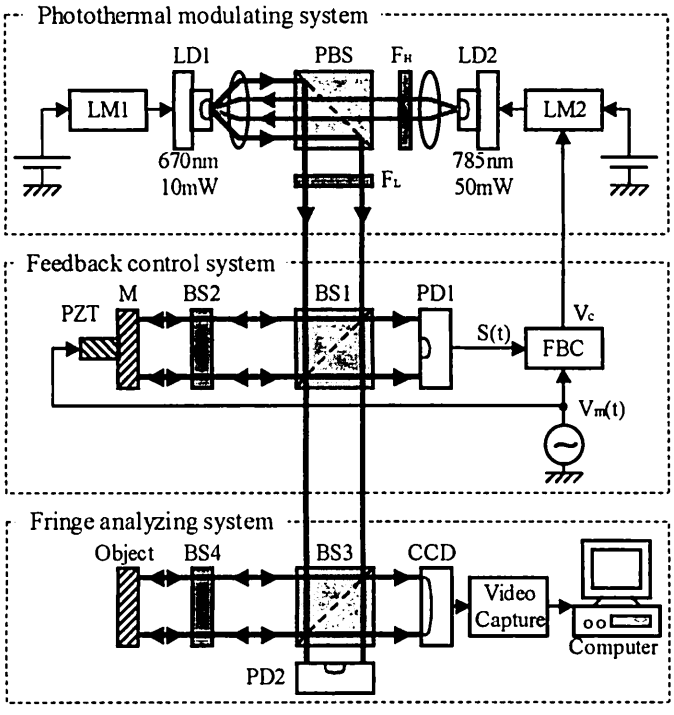

Fig. 17 Phase-locked phase-shifting LD interferometer with photothermal modulation.

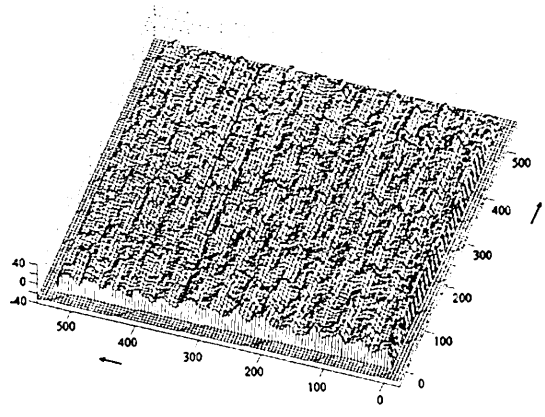

Fig. 18 3-D surface profile measured with phase-locked phase-shifting LD interferometer.

to that in the FB control system. Surface profiles of a diamond-turned aluminum disk whose roughness is ~40nm are shown in Fig. 18. The experimental conditions were λ_1=670 nm, λ_2=785 nm, β=1.87×10^{-4} nm/mA, L_0=60 mm, and $2\pi/\omega_c$=1 kHz, respectively. The error in the phase-shift was estimated to be 5.2×10^{-4} rad, in this experiment.

Similar PSI[10] has been proposed using SFD. The surface profile of a spherical mirror of 130 mm diameter was measured on a wooden table. The parameters in the experiment were λ=689.8 nm, β=4.65×10^{-3} nm/mA, L_0=234 mm, respectively. The result agreed well with that obtained on an optical bench. External disturbance was suppressed to 1/30.

A Fizeau type PSI equipped with an electrical FB loop has been proposed[20]. It uses orthogonally, and linearly polarized two-frequency light beams. The FB signal is given by the phase difference between two beat signals. The parameters in the experiments were λ=633 nm, β=5.76×10^{-3} nm/mA, and L_0=172 mm, respectively. The frequency applied to an acousto-optic cell was 1 MHz. It was concluded that the system has a repeatability of ~λ/60 rms under unstable environmental conditions.

6.2 DISTURBANCE-FREE BUCKET METHOD USING AN FB CONTROL

The PSI requires four fringe images that have a phase difference of π/2 between them. So, it is no easy task to apply, at exactly the right phase on the interference images. In contrast, the integrating-bucket method is convenient, because it merely requires the initial phase of the modulation current and the modulation depth that depends on the amplitude of the modulation current. Parameter adjustments are rather straightforward, compared with those required in PSI. The slow (30 Hz) frame-rate results in a slow modulating current. This leads to the poor response in the FB control because the FB signal is generated with the synchronous detection by using the modulating signal. The setup shown in Fig. 19 enables us to improve the response of the FB control[21] by means of the CCD camera's electronic shutter[22].

Figure 20 illustrates high-speed modulating signal generation. One-quarter period of a conventional modulation signal is equal to a frame rate of T_f=1/30 s. It means that the frequency of the modulation signal is restricted to 7.5 Hz (Fig. 20(a)) because the bucket method requires four images, as shown in Eqs. (21) and (22). On the other hand, if the shutter

function is activated (Fig. 20(b)), the quarter period of the modulation signal is equal to the shutter speed T_s. Thus, modulation frequency f_m is given by

$$f_m = \frac{1}{T_m} = \frac{1}{4T_f}\left\{4 \cdot \text{round}\left[\frac{1}{4}\left(\frac{T_f}{T_s} \mp 1\right)\right] \pm 1\right\}, \quad (30)$$

where round[ ] rounds off the argument.

We set shutter speed and modulation frequency to 106 μs and 2361 Hz, respectively. Modulation frequency was calculated by Eq. (30). The surface profiles of the diamond-turned aluminum disk are shown in Fig. 21. These were measured on a 5-mm-thick iron plate placed on a wooden desk. The wavelength used in this experiment was λ=685 nm. The second measurement shown in Fig. 21(b) was obtained 10 min after the first measurement shown in Fig. 21(a). Cutting pitch and roughness agreed very well with measurements obtained with a Talystep instrument. Repeatability was estimated as 4.2 nm rms for these measurements.

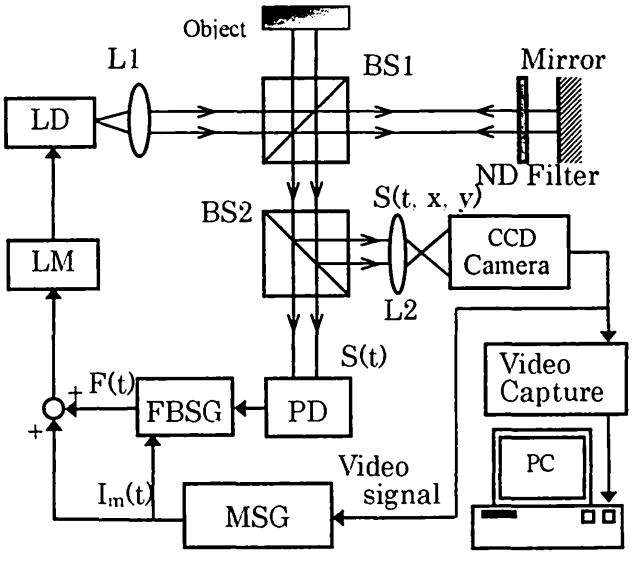

Fig. 19 Disturbance-free high-speed SPM LD interferometer.

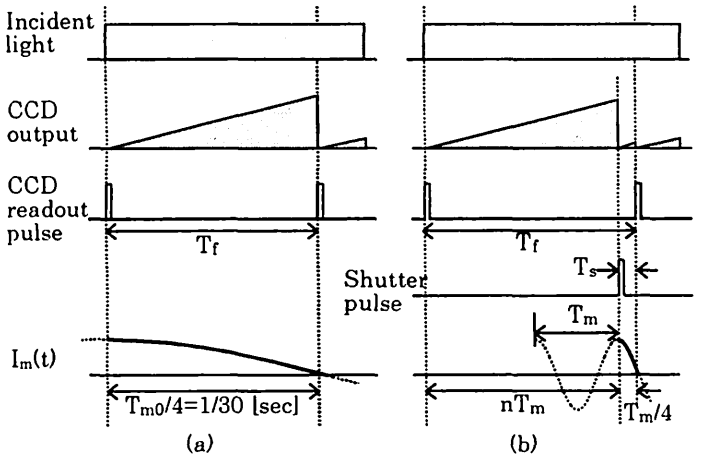

Fig. 20 Schematic of (a) a conventional; modulating signal and (b) a high-speed modulating signal.

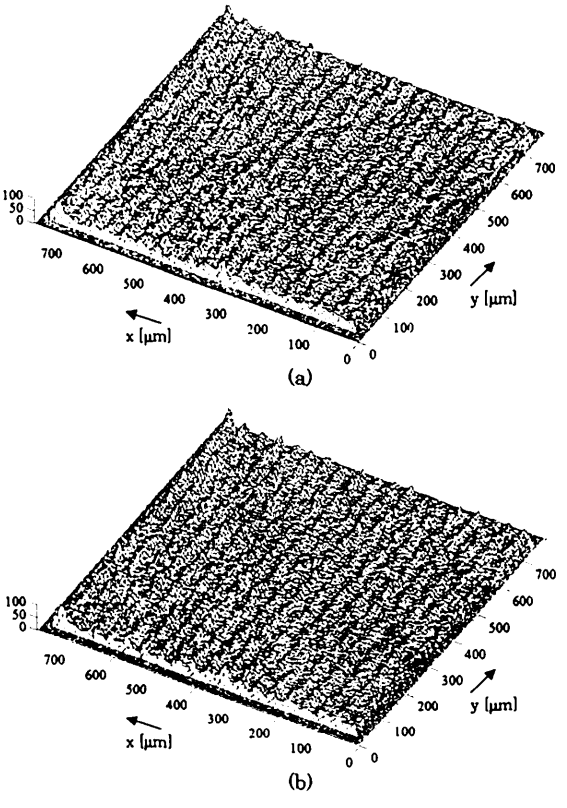

Fig. 21 3-D surface profile of a diamond-turned aluminum disk. Profile (b) was measured 10 min after the first measurement shown in (a).

7. CONCLUSIONS

The principles as well as instances of feedback LD interferometry were summarized. The wavelength tunability of the LD enables us to achieve a so-called 'active' interferometer with a simple electrical circuit. This device uses the phase-locked technique, which is capable of controlling the phase, in such a way as to maintain a constant value. We first explained how to generate the FB signal for three different interferometers. Next, several examples were described for classified targets, such as displacement, surface profile, distance, and disturbance elimination. The most significant results described in this paper are; (a) that the measurable amplitude of the vibration was 2000 nm; (b) that the surface profile of a diamond turned aluminum disk whose roughness was ~100 nm was measured with the phase-locked technique under the repeatability of 10 nm; (c) that the gauge block's step-height (~2 mm) was accurately measured to with a measurement error of 0.16 mm rms; (d) that the surface profile of a diamond turned aluminum disk, whose roughness was ~40 nm, was measured with a repeatability of 4.2 nm rms on wooden desk.

REFERENCES

1. K. Tatsuno and Y. Tsunoda, "Diode laser direct modulation heterodyne interferometer," *Appl. Opt.* **26**, 37-40 (1987).
2. Y. Ishii, J. Chen, and K. Murata, "Digital phase-measuring interferometry with a tunable laser diode," *Opt. Lett.* **12**, 233-235 (1987).
3. T. Yoshino, M. Nara, S. Mnatzakanian, B. S. Lee, and T. C. Strand, "Laser diode feedback interferometer for stabilization and displacement measurement," *Appl. Opt.* **26**, 892-897 (1987).
4. T. Suzuki, O. Sasaki, and T. Maruyama, "Phase-locked laser diode interferometry for surface profile measurement," *Appl. Opt.* **28**, 4407-4410 (1989).
5. T. Suzuki, O. Sasaki, K. Higuchi, and T. Maruyama, "Phase locked laser diode interferometer: high speed feedback control system," *Appl. Opt.* **30**, 3622-3626 (1991).
6. T. Suzuki, O. Sasaki, K. Higuchi, and T. Maruyama, "Differential type of phase locked laser diode interferometer," *Appl. Opt.* **31**, 7242-7248 (1992).
7. O. Sasaki, K. Takahashi, and T. Suzuki, "Sinusoidal phase modulating laser diode interferometer with a feedback control system to eliminate external disturbance," *Opt. Eng.* **29**, 1511-1515 (1990).
8. T. Suzuki, O. Sasaki, and T. Maruyama, "Absolute distance measurement using wavelength-multiplexed phase-locked laser diode interferometry," *Opt. Eng.* **35**, 492-497 (1996).
9. R. Onodera and Y. Ishii, "Frame rate phase-shifting interferometer with a frequency-modulated laser diode," *Opt. Eng.* **38**, 2045-2049 (1999).
10. J. Liu, I. Yamaguchi, J. Kato, and T. Nakajima, "Active phase-shifting interferometer using current modulation of a laser diode," *Opt. Rev.* **4**, 287-292 (1996).
11. I. Yamaguchi, J. Liu, and J. Kato, "Active phase-shifting interferometer for shape and deformation measurements," *Opt. Eng.* **35**, 2930-2937 (1996).
12. J. Chen, Y. Ishii, and K. Murata, "Heterodyne interferometry with a frequency-modulated laser diode," *Appl. Opt.* **27**, 124-128 (1988).
13. T. Suzuki, S. Hirabayashi, O. Sasaki, and T. Maruyama, "Self-mixing type of phase-locked laser diode interferometer," *Opt. Eng.* **38**, 543-548 (1999).
14. T. Suzuki, O. Sasaki, S. Takayama, and T. Maruyama, "Real-time displacement measurement using synchronous detection in a sinusoidal phase modulating interferometer," *Opt. Eng.* **32**, 1033-1037 (1993).

15. T. Suzuki, O. Sasaki, J. Kaneda, and T. Maruyama, "Real-time two-dimensional surface profile measurement in sinusoidal phase modulating laser diode interferometer," *Opt. Eng.* **33**, 2754-2759 (1994).
16. T. Suzuki, T. Okada, O. Sasaki, and T. Maruyama, "Real-time vibration measurement using a feedback type of laser diode interferometer with an optical fiber," *Opt. Eng.* **36**, 2496-2502 (1997).
17. T. Suzuki, T. Muto, O. Sasaki, and T. Maruyama, "Wavelength-multiplexed phase-locked laser diode interferometer using a phase-shifting technique," *Appl. Opt.* **36**, 6196-6202 (1997).
18. T. Suzuki, X. Zhao, and O. Sasaki, "Phase-locked phase-shifting laser diode interferometer with a photothermal modulation," *Appl. Opt.* **40**, 2126-2131 (2001).
19. T. Suzuki, M. Matsuda, O. Sasaki, and T. Maruyama, "Laser-diode interferometer with a photothermal modulation," *Appl. Opt.* **38**, 7069-7075 (1999).
20. M. Yokota, A. Asaka, and T. Yoshino, "Stabilized phase-shifting fringe analysis by use of current frequency modulation of laser diode," *Appl. Opt.* **40**, 5023-5027 (2001).
21. T. Suzuki, T. Maki, X. Zhao, and T. Suzuki, "Disturbance-free high-speed sinusoidal phase-modulating laser diode interferometer," *Appl. Opt.* **41**, 1949-1953 (2002).
22. X. Zhao, T. Suzuki, and O. Sasaki, "Photothermal phase-modulating laser diode interferometer with high-speed feedback control," *Opt. Rev.* **9**, 13-17 (2002).